HHS Public Access

Author manuscript

Ultrasound Med Biol. Author manuscript; available in PMC 2023 March 27.

Published in final edited form as:

Ultrasound Med Biol. 2021 September ; 47(9): 2550–2559. doi:10.1016/j.ultrasmedbio.2021.05.016.

POINT-OF-CARE ULTRASOUND AS A TOOL TO ASSESS WOUND SIZE AND TISSUE REGENERATION AFTER SKIN GRAFTING

YASH MANTRI[*], **JASON TSUJIMOTO**[*], **WILLIAM F. PENNY**[†], **PRANAV S. GARIMELLA**[‡], **CAESAR A. ANDERSON**[§], **JESSE V. JOKERST**[¶, ‖ ,#]

[*]Department of Bioengineering, University of California San Diego, La Jolla, California, USA

[†]Department of Medicine, University of California San Diego, La Jolla, California, USA

[‡]Division of Nephrology—Hypertension, School of Medicine, University of California San Diego, La Jolla, CA, USA

[§]Department of Emergency Medicine, Hyperbaric Medicine and Wound Healing Center, University of California San Diego, Encinitas, California, USA

[¶]Department of NanoEngineering, University of California San Diego, La Jolla, California, USA

[‖] Materials Science Program, University of California San Diego, La Jolla, California, USA

[#]Department of Radiology, University of California San Diego, La Jolla, California, USA

Abstract

Chronic wounds can be difficult to heal and are often accompanied by pain and discomfort. Multiple skin substitutes or cellularized/tissue-based skin products have been used in an attempt to facilitate closure of complex wounds. Allografts from cadaveric sources have been a viable option in achieving such closure. However, early assessment of graft incorporation has been difficult clinically, often with delayed evidence of failure. Visual cues to assess graft integrity have been limited and remain largely superficial at the skin surface. Furthermore, currently used optical imaging techniques can penetrate only a few millimeters deep into tissue. Ultrasound (US) imaging offers a potential solution to address this limitation. This work evaluates the use of US to monitor wound healing and allograft integration. We used a commercially available dual-mode (US and photoacoustic) scanner operating only in US mode. We compared the reported wound size from the clinic with the size measured using US in 45 patients. Two patients from this cohort received an allogenic skin graft and underwent multiple US scans over a 110-d period. All data were processed by two independent analysts; one of them was blinded to the study. We measured change in US intensity and wound contraction as a function of time. Our results revealed a strong correlation (R^2 = 0.81, p < 0.0001) between clinically and US-measured wound sizes. Wound contraction >91% was seen in both patients after skin grafting. An inverse relationship between

Address correspondence to Jesse V. Jokerst, Department of NanoEngineering, University of California San Diego, La Jolla, CA 92093, USA. jjokerst@ucsd.edu.

Conflict of interest disclosure—There are no conflicts of interest to declare.

SUPPLEMENTARY MATERIALS

Supplementary material associated with this article can be found in the online version at doi:10.1016/j.ultrasmedbio.2021.05.016.

wound size and US intensity ($R^2 = 0.77$, $p < 0$ .0001) indicated that the echogenicity of the wound bed increases as healthy cells infiltrate the allograft matrix, regenerating and leading to healthy tissue and re-epithelization. This work indicates that US can be used to measure wound size and visualize tissue regeneration during the healing process.

Keywords

Point of care ultrasound imaging; Chronic wound care; Cellularized/tissue-based skin products; Skin grafts; Tissue regeneration and wound sizing

INTRODUCTION

Wound healing is one of the most complex processes in the human body (Tottoli et al. 2020). An ideally healed wound is an area that has been restored to normal anatomy, structure, functionality and appearance after an injury (Tottoli et al. 2020). Wounds can be classified into two broad categories, acute and chronic, depending on underlying cause and how long they take to heal. An acute wound is a sudden injury to the skin that heals predictively within 8–12 wk (Martin and Nunan 2015). A chronic wound occurs because of a prolonged inflammatory response during healing that is difficult to heal, lasts longer than 12 wk and frequently recurs (Martin and Nunan 2015). Poor perfusion into the wound site can significantly impair wound healing (Holmer et al. 2018). Access to expert wound care centers can promote evidence-based wound care, leading to 45% faster healing rates and a more efficient use of health resources (Edwards et al. 2013; Innes-Walker et al. 2019).

There are several wound treatment modalities. Standard wound care elements include serial debridement, compression therapy and judicious use of various wound dressings to control moisture balance, along with antimicrobial efforts to optimize the wound bed for successful healing (Vinkel et al. 2020). These efforts also include minimizing pressure forces while optimizing vascular status of the affected limb. Several additional advanced adjunctive modalities exist. Negative-pressure wound therapy devices, adjunctive hyperbaric oxygen therapy and cellularized/tissue-based skin products are viable options (Greer et al. 2013). Cellularized/tissue-based skin products or bio-engineered skin grafts made of synthetic and/or biological materials are often used as aids to promote wound closure and restore skin function (Augustine et al. 2014; Tottoli et al. 2020). The allograft skin substitutes provide a scaffold to the open wound defect. This scaffold will then become colonized by host immune cells as the healing cascade progresses. Clinicians often refer to the process of graft integration with the recipient area as “taking.” Healthy host cells infiltrate the allograft matrix. These cells then differentiate into regenerated tissue, ultimately integrating with surrounding healthy host tissue in a seamless fashion. Allograft take is typically dependent on the integrity of a healthy granular host wound base (Adams and Ramsey 2005; Andreassi et al. 2005) A negative immune response, infection, excessive exudation and compromised hemostasis can all endanger the survival of the allograft. Obstruction of adherence to granulating tissue and penetration of neocapillaries can occur (Adams and Ramsey 2005; Benichou et al. 2011). Currently, clinicians rely on clinical experience and visual cues such as graft color, odor, texture, edema, drainage and necrosis to monitor the graft and

the underlying wound health (Zamfirescu et al. 2009; Ren et al. 2020) However, visual inspection is limited to the skin surface whereas underlined edema and graft detachment can go unnoticed. Furthermore, studies have reported extensive heterogeneity in wound evaluations between different health care professionals (Stremitzer et al. 2007; Gartlan et al. 2010). One study compared how nurses and clinicians evaluated one diabetic ulcer—there was significant discordance in wound evaluation, with 62.5% describing the wound as reddened in contrast to 37.5% reporting the same wound as bland. Similar discordance was noted in their ability to quantify wound exudate, with 62.5% describing exudate as moderate, 25% reporting no exudate and 12.5% indicating that exudate could not be specified (Stremitzer et al. 2007). This underscores the necessity for a more objective wound assessment system that avoids such an observational variation.

Imaging is an indispensable tool used to see what the eye cannot (Dargaville et al. 2013). Digital imaging using standard cameras has helped size wounds more accurately and follow clinical progress after grafting (Quan et al. 2007; Papazoglou et al. 2010). Ultraviolet light can visualize hidden wound features and has helped the field of forensics (Barsley et al. 1990). Spectral imaging and two-photon fluorescence microscopy have shown promise in visualizing vasculature and measure oxygen saturation in animal models; both are key parameters for optimal graft health (Yudovsky et al. 2010; Yanez et al. 2013; Kennedy et al. 2019; Schmidt et al. 2021). Fluorescence imaging has also been used to detect bacterial infection in chronic wounds (Rennie et al. 2017). Unfortunately, all these techniques are optical and, thus, are limited by the penetration depth of light through tissue (approx 100 μm) while chronic wounds can exist much deeper (≤2 cm) (Wilson and Adam 1983; Stremitzer et al. 2007). X-Ray or magnetic resonance imaging can be used to look deeper into diseased tissue but these either lack soft tissue contrast and risk radiation exposure (X-ray) or are expensive, cannot be point-of-care and lack resolution (magnetic resonance imaging).

Ultrasound (US) imaging is a unique imaging modality that solves all these major limitations. It is a quick, inexpensive, non-radiative, non-invasive and point-of-care imaging modality that can look deep into soft tissue (≤10 cm) (Ng and Swanevelder 2011; Szabo and Lewin 2013). The use of US as a therapeutic tool to aid debridement and promote healing has been widely reported but there are very few reports on the use of US imaging to monitor wound healing (Kavros et al. 2007; Driver and Fabbi 2010; Ennis et al. 2011). A recent small case series reported that US, Doppler and elastography could be used to determine wound morphology, biomechanics and proximity to other anatomical structures such as bone and tendon (Henshaw et al. 2020). Another case study of a 46-y-old woman with a stage IV sacral pressure ulcer revealed that multiple 2-D US images could be reconstructed for 3-D visualization of the ulcer (Yabunaka et al. 2015). Photoacoustic imaging and high-resolution harmonic US have also been used to stage and track healing of pressure ulcers and burn wounds in animal models (Gnyawali et al. 2015; Hariri et al. 2019). Although these studies depict the advantages of US imaging such as deeper imaging and elastography, a longitudinal human clinical study monitoring wound healing has not yet been reported. The ability to monitor a skin graft as it integrates would have high clinical significance and allow clinicians to make more informed therapeutic decisions. This work aims to evaluate the use of US to monitor wound healing and allograft integration.

METHODS

Patients

This study was approved by the Human Research Protections Program at the University of California, San Diego (Institutional Review Board No. 191998 and 202019X). Informed written consent from each patient was acquired before scanning. The inclusion criteria were as follows: (i) Ulcers could not be larger than 15 cm^2 in area; (ii) patients had to be ≥18 y and able to provide consent. Exclusion criteria included (i) presence of a bloodborne pathogen; (ii) presence of other lesions (*e. g.,* melanomas) at the wound site; (iii) presence of orthopedic implants; (iv) wounds between digits or in the pubic region. Sixty-three patients (65 wounds) were recruited for this study. Table 1 describes the patient demographic distribution. All patients were imaged.

Two patients (patients A and B) who received allogenic skin grafts underwent multiple follow-up scans over a period of 110 d. Patient A was a 77-y-old non-diabetic woman with a history of hypothyroidism. Patient A presented with an open, chronic, post-operative left knee wound with tendon involvement and chronic venous hypertension on both sides. Patient A was first scanned 103 d after presentation, followed by 13 follow-up scans over a 110-d period. Patient B was a 33-y-old non-diabetic man with a history of renal transplant. Patient B presented with a left, anterior, lower limb, posttraumatic ulcer with chronic venous hypertension on the left side. Patient B was first scanned 33-d after presentation followed by 10 follow-up scans over a 106-d period.

This study did not involve any additional visits and was performed during a regularly scheduled wound care visit. The frequency of visits was independently decided by the wound specialist (C.A.A.) depending on the patient's needs. The wound site was prepared by removing any dressings and cleaning with sterile saline before scanning. Neighboring tissue was further cleaned using alcohol swabs to prevent infection. A photograph with a wound ruler was also taken to correctly size the wound surface. To prevent cross-contamination and infections, we used a new sterile CIV-Flex transducer cover for every scan (No. 921191, AliMed Inc., Dedham, MA, USA).

US imaging

We used a commercially available LED-based photoacoustic/US imaging system (AcousticX from Cyberdyne Inc., Tsukuba, Japan) (Hariri et al. 2018). In this study, we used only the ultrasound mode. The US transducer has 128 linearly arranged elements operating with a central frequency of 7 MHz, bandwidth of 80.9% and field of view of 4 cm. Sterile US gel (Aquasonic 100, Parker Laboratories Inc., Fairfield, NJ, USA) and a custom hydrophobic gel pad from Cyberdyne Inc. were used for US coupling between the transducer and skin surface. All US images were acquired at 30 frames/s.

Wounds smaller than 5 cm in length (patient A) were scanned in a single sweep from inferior healthy tissue over the wound to superior healthy tissue. From these scans, we selected representative frames for inferior healthy tissue, two wound sites (sites i and ii) and superior healthy tissue. For large wounds (patient B), we selected three wound sites at discrete distances from the inferior wound edge and tracked wound progression over time

(Fig. 1a). Sites inferior and superior to the wound were used as healthy controls. To monitor tissue regeneration, we measured changes in US intensity (mean gray value) and change in wound size as a function of time. All images were acquired by Y.M. only. It is important to note that all US scans were performed by hand. Thus, it is impossible to perfectly match US frames from the same site over multiple imaging sessions. To reduce the effects of this limitation, we matched the underlying bone morphology to compare similar spots over time. Patients with skin grafts went through the same imaging protocol with no added steps.

Image processing

All US frames were reconstructed and visualized using the custom software built for the AcousticX photoacoustic imaging system developed by Cyberdyne Inc. (Version 2.00.10). B-Mode, coronal cross-section images were exported as 8-bit gray-scale images. The images were further processed to measure wound width, area and US intensity using Fiji, an ImageJ extension, Version 2.1.0/1.53c (Schindelin et al. 2012). Data was plotted using Prism Version 9.0.0. All measurements were made using custom region-of-interest (ROI) analysis for individual frames. Drawing ROIs by hand can be very subjective. Hence, all image quantification was independently confirmed by two analysts (Y.M. and J. T.). J.T. was blinded to the study and only received B-mode US images to analyze the data.

To corroborate our method with the current gold standard eye measurements we compared reported wound size with size measured with US imaging. The reported wound size was provided by C.A.A. and his nursing team and was recorded as part of standard care. The wound width under US was measured using custom ROI analysis to outline the wound on a single frame. Wound width was defined as the widest region within the wound ROI (Fig. 1b).

We quantified changes in US intensity over time in a constant ROI. A custom ROI (outline of wound site) was drawn for patients A and B on day 1, and the US intensity within that ROI was tracked over time. Maintaining a constant ROI allows us to quantify tissue regeneration as the graft integrates into the wound bed. To further compare US intensity between wounded and healthy tissue, a dynamic baseline US intensity for healthy tissue was measured. We measured the mean gray value and its standard deviation (0.5 × 0.5 cm ROI) in two frames representing inferior and superior healthy tissue, for each time point. The healthy window was defined within one standard deviation of the dynamic baseline. US intensities falling under and over this window were considered as wound and scar tissue, respectively.

Finally, we monitored change in wound area under the skin graft. Custom ROIs were drawn for individual sites at each imaging time point. An area was considered to be a wound if its US intensity was significantly below the healthy window defined above.

Statistical testing

A Bland–Altman analysis was used to look for bias between clinically reported wound (gold standard) and US-measured wound width. A mean bias >0.06 cm would be considered clinically significant as the lateral resolution of the US transducer ranges from 0.05–0.06 cm (Hariri et al. 2018).

To reduce the subjective nature of ROI-based analysis, two independent analysts, Y.M. and J.T. processed all the images. J.T. was blinded to the study. A Bland–Altman analysis was used to look for systemic bias between two independent analyses of the same images. For US intensity measurements, a mean bias above 17 gray-scale values (standard deviation in healthy tissue) would be considered clinically significant. For wound area measurements, a mean bias greater than 5% of the largest wound size would be considered clinically significant.

RESULTS

Figure 1a is a typical US scan over a wound site. We illustrate that US imaging can be used to reliably size wounds only limited by the width of the transducer. Skin graft integration, tissue regeneration and changes in wound size can be easily visualized and quantified using US, which is not possible by eye. We also found that there is a significant negative correlation ($R^2 = 0.77$, $p < 0.0001$) between wound size and US intensity.

Wound dimensions

Of the cohort of 63 patients with 65 wound sites, 20 wounds could not be sized with US: 15 wounds did not have a reported wound size from the clinic and were excluded; 5 wounds were located in regions with high curvature such as the lateral side of the toe or ankle, which makes US coupling difficult in these regions with a linear array transducer. Hence, 45 wounds were used to compare reported wound size with the US-measured size. Figure 1c illustrates that there is a strong correlation ($R^2 = 0.81$, $p < 0.0001$) between reported and measured wound widths. A Bland–Altman analysis was used to check for any bias between the gold standard eye measurements and our US imaging technique (Supplementary Fig. S1, online only). A calculated mean bias of −0.05 cm rejected our null hypothesis of clinical significance above 0.06 cm.

Wound regeneration after skin grafting

Figure 2a–c depicts the wound progression, and Figure 2d, the imaging and intervention/treatment timeline for patient A. Figure 2e–g depicts the wound progression, and Figure 2h the imaging and intervention/treatment timeline, for patient B.

Patient A

Patient A had a left knee ulceration and underwent 13 US scans over 110 d. Patient A received a human cadaver-derived, acellular dermal matrix (AlloDerm, Lifecell, Branchburg, NJ, USA) skin graft 28 d before the first scan. A second tissue matrix allograft composed of dehydrated human amnion/chorion membrane (Epi-Fix, MiMedx, Marietta, GA, USA) was used 75 d after the first scan. Supplementary Figures S2 and S3 (online only) illustrate the visual and US scan progression over two wounds and one healthy site. Imaging sites are marked i, ii and healthy from inferior–superior regions. Wound pictures (Fig. 2a–c) show wound contraction and skin graft integration at the surface over time. An increase in tissue echogenicity is seen at both sites i and ii and is indicative of skin graft integration (Supplementary Fig. S2, online only). The superior healthy control tissue remains unchanged over the study period.

Figure 3c–f quantifies the US data for patient A. The dynamic baseline for healthy tissue was measured over 13 independent scans (73.5 ± 12.9 [unique for patient A]). Changes in US intensity over time for sites i and ii indicated that it took 90 d for site i and 96 d for site ii to achieve gray-scale values similar to those of healthy tissue (Fig. 3c, 3e). Wound size under the skin graft exhibited varied rates of contraction for both sites. Site i had an 89.2% reduction and site ii a 96.0% reduction in size over 110 d (Fig. 3d, 3f). Wound contraction was slowest between days 14 and 68, which is consistent with the physician notes reporting slow improvements and signs of edema during the same period. Interestingly, wound contraction was fastest between days 68 and 90, which was also noted by the attending doctor.

Patient B

Patient B was a 33-y-old man with an anterior, lower left limb ulceration who underwent 10 US scans over a 106-d period. Patient B received a human cadaver-derived, acellular dermal matrix (AlloDerm, Lifecell, Branchburg, NJ, USA) skin graft 49 d after the first scan. We monitored wound progression at three wound sites: i, ii and iii (inferior, medial and superior, respectively). Figure 4 illustrates the differences between wound and healthy tissue while focusing on site ii and a superior healthy control only. Annotated images on sites i and iii can be found in the Supplementary Data (Supplementary Figs. S4 and S5, online only).

The average healthy gray-scale value measured over 10 separate scans was 90.4 ± 21.5 (unique for patient B). All wound sites exhibited an increase in wound size and loss of US signal until skin grafting followed by a tissue regeneration and wound contraction period (Supplementary Fig. S4). Healthy control tissue remained unchanged over the same period. Sites i and ii responded differently than site iii (Fig. 3g–l). Between days 1 and 62, the wound area at site i increased from 0.37 to 1.42 cm^2 while that at site ii increased from 0.20 to 1.10 cm^2. Both sites i and ii exhibited an increase in wound size and tissue loss up to 62 d into the study even though patient B was skin grafted on day 49 (Fig. 3h, 3j). Site iii responded to treatment at a different rate. Wound area at site iii increased from 0.05 to 1.23 cm^2 within the first 42 d, followed by a healing period. By the end of the study, sites i, ii and iii exhibited 86.1%, 78.6% and 91.7% contraction, respectively. Photographs clearly indicate that patient B's wound had not completely healed by the end of the study (Fig. 4m). Incomplete healing can be seen when US intensity is monitored over time (Fig. 3g–k). The measured US intensities approach the healthy window but do not exhibit complete regeneration after 110 d of treatment.

A plot of wound area versus US intensity revealed an inverse relationship between the two variables, with R^2 = 0.77 and 0.72 for patients A and B, respectively. A large wound with less tissue had low US signal while a small wound with regenerated tissue had high US signal (Fig. 5).

All data quantification was done by two independent analysts (Y.M. and J.T.). J.T. was blinded to the study while Y.M. acquired and analyzed all the data. Bland–Altman analysis revealed no significant bias between the two analysts. For US intensity measurements, a mean bias of 4.12 gray values between the two analysts rejected our null hypothesis of clinical significance above 17 gray values (standard deviation in healthy tissue). For wound

area measurements, a mean bias of 0.10 cm^2 (4.4% of largest measured wound size) rejected our null hypothesis of clinical significance above 5% of the largest measured area.

DISCUSSION

The fast, inexpensive, reliable and pain-free characteristics of point-of-care US imaging make it an ideal modality for monitoring wound progression. Currently, wounds are sized by eye using a wound ruler as reference. Although more advanced sizing protocols using high-definition cameras with complex edge detection and neural networks have been reported, their limited penetration into tissue makes depth measurements difficult (Chino et al. 2020; Malone et al. 2020; Toygar et al. 2020). Furthermore, wounds may prematurely contract at the surface level only ahead of a voluminous deeper cavity defect (Medina et al. 2005). This dimension is often neglected though it may further explain aberrant wound healing delays or cause of wound deterioration. The ability of US to non-invasively image under the skin surface makes it an ideal imaging modality to solve such limitations. Figure 1c illustrates that wound width measured using US imaging is strongly correlated ($R^2 = 0.81$) with the reported eye-measured values. Bland–Altman analysis also revealed no clinically significant difference between reported and measured values (Supplementary Fig. S1). One limitation is that wounds >4 cm in width are consistently undersized. This is because the US transducer used in this study has 128 elements, each measuring 3.5 mm in length with a pitch of 0.3 mm, yielding a lateral field of view of ~4 cm (Hariri et al. 2018), US imaging has value in estimating wound depths, but these are usually difficult to measure by eye and hence are rarely reported.

Tissue loss or edema accumulation results in hypoechoic regions on US images (Terslev et al. 2003; Ripollés et al. 2013). On the other hand, scar tissue and edema reduction caused by the use of compression modalities results in hyperechoic regions (Ackerman et al. 2019). Patients have unique soft tissue density and collagen arrangements, giving them unique baseline acoustic properties. It is important to measure healthy tissue US intensity separately for each case to distinguish between diseased, healthy and scar tissue. With skin grafts, the ideal outcome is restoration of anatomical continuity along with functionality while minimizing scarring. US imaging is an effective tool for visualizing tissue regeneration because US intensity increases as the wound heals. This phenomenon is clearly visible with both patients A and B. Figure 3 illustrates the change in US intensity and wound size over time. It is interesting to note there was an inverse relationship between wound size and US intensity for both patients (Fig. 5). In both patients, the corresponding US intensity increased whenever wound size decreased. This is because healthy cells infiltrate into the graft matrix regenerating healthy tissue as the skin graft takes; this, in turn, increases US signal. Skin grafting did not lead to scar formation because the US intensity of regenerated tissue stayed within the defined healthy tissue window (Fig. 3c, 3e, 3g, 3i, 3k). A high-collagen orientation index in scar and keloid tissue leads to hyperechogenicity under US imaging (Timar–Banu et al. 2001; Verhaegen et al. 2009).

Sometimes wounds deteriorate secondary to a deeper unhealed voluminous defect. This defect often collects fluid and may evolve into a seroma or an abscess (Landis 2008). Such a defect is particularly difficult to predict and visualize with current methods at the bedside.

Therefore, visual clinical cues such as erythema, swelling, fluctuance and/or presence of pain can be used to predict tissue health under the skin (Ren et al. 2020). US imaging is especially effective in providing insight into deeper wound elements. The real-time, high-resolution, high-depth penetration nature of US allows it to detect signs of edema and tissue loss before it is visible on the skin surface. The ability of US to predict tissue loss is seen in patient B (Fig. 4), where site ii exhibits signs of tissue loss approximately 0.5 cm under the wound surface on day 1 (Fig. 4b; Supplementary Fig. S4, online only). The hypo-echoic regions between the tibia and the US probe cover in Figure 4e and 4h are indicative of further tissue loss, which left the tibia exposed by day 42. The increase in wound size and loss of tissue were also corroborated by image analysis (Fig. 3g–l) where US intensity decreases and wound area increases over the first 62 d.

Wound healing is an extremely complicated process that is affected by many variables such as age, local perfusion, moisture and patient compliance (Valencia et al. 2001; Guo and DiPietro 2010). Younger patients are more likely to heal faster than older patients (Gould et al. 2020). Comparison of the healing rates between patient A (77-y-old) and patient B (33-y-old) in Figure 3 reveals that patient B exhibited faster wound contraction after skin grating compared with patient A. Patient A had 62% contraction within 103 d of the first skin graft placement. Patient B had a larger wound but 65% contraction within 42 d of skin grafting. Furthermore, patient A required a secondary skin graft (EpiFix, MiMedx, Marietta, GA, USA) 54 d into the study after which the wound contraction rate increased at both sites (Fig. 3c–f). These results suggest that US imaging could be used to evaluate wound healing rate; however, a more comprehensive and well-powered study is needed to draw conclusions.

Although US imaging is a powerful tool for monitoring wound health, it has its limitations. US images are gray-scale images, and it is difficult to distinguish between wound sites responding to treatment and the surrounding healthy tissue. Furthermore, US images can provide high-resolution structural imaging but lack functional imaging capabilities (Kim et al. 2020). Photoacoustic imaging is similar to US but uses light as an excitation source to produce pressure waves (Mantri and Jokerst 2020). It has already shown promise in visualizing ulcers and neovascularization in mice (Hariri et al. 2019), which is key for wound healing and skin graft integration. Our future work will look to incorporate photoacoustic imaging to monitor neovascularization in human subjects.

CONCLUSIONS

US imaging is a valuable tool for studying skin graft integration used for chronic wound treatment. We first found that wound width measurements made by US imaging are strongly correlated to measurements made visually. Second, a thorough investigation in two patients (five wound sites), both receiving allogenic skin grafts, revealed that wound contraction, healing and skin graft integration could be monitored using wound area and US intensity. The loss of tissue and inflammation resulted in hypo-echoic regions on US which healed after skin graft placement and integration in both patients. Over 110 d, patient A exhibited up to 96% wound contraction, whereas patient B exhibited up to 91.7% contraction over a similar period. During the healing process, US intensities recovered into the healthy tissue window showing soft tissue regeneration under the skin graft.

Supplementary Material

Refer to Web version on PubMed Central for supplementary material.

Acknowledgments—

Figure 1A was created with BioRender.com. We acknowledge support from the National Institutes of Health through Grant 1R21AG065776–01, as well as internal funds from the University of California, San Diego, under the Galvanizing Engineering in Medicine program. Y.M. acknowledges help from Brandon Brodish, RN, Luz Amezquita, RN, Starr Nimeth, LVN, and the entire team at the Hyperbaric Medicine and Wound Healing Center, University of California San Diego, Encinitas, California, USA.

REFERENCES

Ackerman JE, Studentsova V, Myers M, Buckley MR, Richards MS, Loiselle AE. Non-invasive ultrasound quantification of scar tissue volume identifies early functional changes during tendon healing. J Orthop Res 2019;37:2476–2485. [PubMed: 31231903]

Adams DC, Ramsey ML. Grafts in dermatologic surgery: Review and update on full-and split-thickness skin grafts, free cartilage grafts, and composite grafts. Dermatol Surg 2005;31:1055–1067. [PubMed: 16042930]

Andreassi A, Bilenchi R, Biagioli M, D'Aniello C. Classification and pathophysiology of skin grafts. Clin Dermatol 2005;23:332–337. [PubMed: 16023927]

Augustine R, Kalarikkal N, Thomas S. Advancement of wound care from grafts to bioengineered smart skin substitutes. Prog Biomater 2014;3:103–113. [PubMed: 29470769]

Barsley RE, West MH, Fair JA. Forensic photography: Ultraviolet imaging of wounds on skin. Am J Forensic Med Pathol 1990;11:300–308. [PubMed: 2275466]

Benichou G, Yamada Y, Yun SH, Lin C, Fray M, Tocco G. Immune recognition and rejection of allogeneic skin grafts. Immunotherapy 2011;3:757–770. [PubMed: 21668313]

Chino DY, Scabora LC, Cazzolato MT, Jorge AE, Traina C Jr, Traina AJ. Segmenting skin ulcers and measuring the wound area using deep convolutional networks. Comput Methods Programs Biomed 2020;191 105376. [PubMed: 32066047]

Dargaville TR, Farrugia BL, Broadbent JA, Pace S, Upton Z, Voelcker NH. Sensors and imaging for wound healing: A review. Biosensors Bioelectron 2013;41:30–42.

Driver VR, Fabbi M. Recent advances in the use of ultrasound in wound care. Adv Wound Care 2010;1.

Edwards H, Finlayson K, Courtney M, Graves N, Gibb M, Parker C. Health service pathways for patients with chronic leg ulcers: Identifying effective pathways for facilitation of evidence based wound care. BMC Health Services Res 2013;13:86.

Ennis WJ, Lee C, Plummer M, Meneses P. Current status of the use of modalities in wound care: Electrical stimulation and ultrasound therapy. Plast Reconstruct Surg 2011;127:93S–102S.

Gartlan J, Smith A, Clennett S, Walshe D, Tomlinson-Smith A, Boas L, Robinson A. An audit of the adequacy of acute wound care documentation of surgical inpatients. J Clin Nurs 2010;19:2207–2214. [PubMed: 20659200]

Gnyawali SC, Barki KG, Mathew-Steiner SS, Dixith S, Vanzant D, Kim J, Dickerson JL, Datta S, Powell H, Roy S. High-resolution harmonics ultrasound imaging for non-invasive characterization of wound healing in a pre-clinical swine model. PLoS One 2015;10 e0122327. [PubMed: 25799513]

Gould LJ, Abadir PM, White-Chu EF. Age, frailty, and impaired wound healing. In: Rosenthal R, Zenilman M, Katlic M, (eds). Principles and practice of geriatric surgery Cham: Springer; 2020. p. 465–482.

Greer N, Foman NA, MacDonald R, Dorrian J, Fitzgerald P, Rutks I, Wilt TJ. Advanced wound care therapies for nonhealing diabetic, venous, and arterial ulcers: A systematic review. Ann Intern Med 2013;159:532–542. [PubMed: 24126647]

Sa Guo, DiPietro LA. Factors affecting wound healing. J Dent Res 2010;89:219–229. [PubMed: 20139336]

Hariri A, Lemaster J, Wang J, Jeevarathinam AS, Chao DL, Jokerst JV. The characterization of an economic and portable LED-based photoacoustic imaging system to facilitate molecular imaging. Photoacoustics 2018;9:10–20. [PubMed: 29234601]

Hariri A, Chen F, Moore C, Jokerst JV. Noninvasive staging of pressure ulcers using photoacoustic imaging. Wound Repair Regen 2019;27:488–496. [PubMed: 31301258]

Henshaw FR, Reid IB, Spencer AM, Turner DE. Point of care ultrasound imaging as a wound assessment tool in diabetic foot ulcers: a case series. J Wound Care 2020;29:S28–S34.

Holmer A, Marotz J, Wahl P, Dau M, Kämmerer PW. Hyperspectral imaging in perfusion and wound diagnostics—Methods and algorithms for the determination of tissue parameters. Biomed Tech (Berl) 2018;63:547–556. [PubMed: 30028724]

Innes-Walker K, Parker C, Finlayson K, Brooks M, Young L, Morley N, Maresco-Pennisi D, Edwards H. Improving patient outcomes by coaching primary health general practitioners and practice nurses in evidence based wound management at on-site wound clinics. Collegian 2019;26:62–68.

Kavros SJ, Miller JL, Hanna SW. Treatment of ischemic wounds with noncontact, low-frequency ultrasound: The Mayo clinic experience, 2004–2006. Adv Skin Wound Care 2007;20:221–226. [PubMed: 17415030]

Kennedy GT, Stone R, Kowalczewski AC, Rowland RA, Chen JH, Baldado ML, Ponticorvo A, Bernal NP, Christy RJ, Durkin AJ. Spatial frequency domain imaging: A quantitative, noninvasive tool for in vivo monitoring of burn wound and skin graft healing. J Biomed Opt 2019;24 071615. [PubMed: 31313538]

Kim J, Park EY, Park B, Choi W, Lee KJ, Kim C. Towards clinical photoacoustic and ultrasound imaging: Probe improvement and real-time graphical user interface. Exp Biol Med 2020;245:321–329.

Landis SJ. Chronic wound infection and antimicrobial use. Adv Skin Wound Care 2008;21:531–540. [PubMed: 18981758]

Malone M, Schwarzer S, Walsh A, Xuan W, Al Gannass A, Dickson HG, Bowling FL. Monitoring wound progression to healing in diabetic foot ulcers using three-dimensional wound imaging. J Diabetes Complications 2020;34 107471. [PubMed: 31859145]

Mantri Y, Jokerst JV. Engineering plasmonic nanoparticles for enhanced photoacoustic imaging. ACS Nano 2020;14:9408–9422. [PubMed: 32806027]

Martin P, Nunan R. Cellular and molecular mechanisms of repair in acute and chronic wound healing. Br J Dermatol 2015;173:370–378. [PubMed: 26175283]

Medina A, Scott PG, Ghahary A, Tredget EE. Pathophysiology of chronic nonhealing wounds. J Burn Care Rehabil 2005;26:306–319. [PubMed: 16006837]

Ng A, Swanevelder J. Resolution in ultrasound imaging. Contin Educ Anaesth Crit Care Pain 2011;11:186–192.

Papazoglou ES, Zubkov L, Mao X, Neidrauer M, Rannou N, Weingarten MS. Image analysis of chronic wounds for determining the surface area. Wound Repair Regener 2010;18:349–358.

Quan SY, Lazarus GS, Kohli AR, Kapoor R, Margolis DJ. Digital imaging of wounds: Are measurements reproducible among observers?. Int J Lower Extremity Wounds 2007;6:245–248.

Ren SY, Liu YS, Zhu GJ, Liu M, Shi SH, Ren XD, Hao YG, Gao RD. Strategies and challenges in the treatment of chronic venous leg ulcers. World J Clin Cases 2020;8:5070–5085. [PubMed: 33269244]

Rennie M, Lindvere-Teene L, Tapang K, Linden R. Point-of-care fluorescence imaging predicts the presence of pathogenic bacteria in wounds: A clinical study. J Wound Care 2017;26:452–460. [PubMed: 28795890]

Ripollés T, Rausell N, Paredes JM, Grau E, Martínez MJ, Vizuete J. Effectiveness of contrast-enhanced ultrasound for characterisation of intestinal inflammation in Crohn's disease: A comparison with surgical histopathology analysis. J Crohn's Colitis 2013;7:120–128. [PubMed: 22483566]

Schindelin J, Arganda-Carreras I, Frise E, Kaynig V, Longair M, Pietzsch T, Preibisch S, Rueden C, Saalfeld S, Schmid B. Fiji: An open-source platform for biological-image analysis. Nat Methods 2012;9:676–682. [PubMed: 22743772]

Schmidt A, Niener F, von Woedtke T, Bekeschus S. Hyperspectral imaging of wounds reveals augmented tissue oxygenation following cold physical plasma treatment in vivo. IEEE Trans Radiat Plasma Med Sci 2021;5:412–419.

Stremitzer S, Wild T, Hoelzenbein T. How precise is the evaluation of chronic wounds by health care professionals?. Int Wound J 2007;4:156–161. [PubMed: 17651230]

Szabo TL, Lewin PA. Ultrasound transducer selection in clinical imaging practice. J Ultrasound Med 2013;32:573–582. [PubMed: 23525382]

Terslev L, Torp-Pedersen S, Savnik A, Von der Recke P, Qvistgaard E, Danneskiold-Samsøe B, Bliddal H. Doppler ultrasound and magnetic resonance imaging of synovial inflammation of the hand in rheumatoid arthritis: A comparative study. Arthritis Rheum 2003;48:2434–2441. [PubMed: 13130462]

Timar-Banu O, Beauregard H, Tousignant J, Lassonde M, Harris P, Viau G, Vachon L, Levy E, Abribat T. Development of noninvasive and quantitative methodologies for the assessment of chronic ulcers and scars in humans. Wound Repair Regener 2001;9:123–132.

Tottoli EM, Dorati R, Genta I, Chiesa E, Pisani S, Conti B. Skin wound healing process and new emerging technologies for skin wound care and regeneration. Pharmaceutics 2020;12:735. [PubMed: 32764269]

Toygar I, Simsir IY, Cetinkalp S. Evaluation of three different techniques for measuring wound area in diabetic foot ulcers: A reproducibility study. J Wound Care 2020;29:518–524. [PubMed: 32924818]

Valencia IC, Falabella A, Kirsner RS, Eaglstein WH. Chronic venous insufficiency and venous leg ulceration. J Am Acad Dermatol 2001;44:401–424. [PubMed: 11209109]

Verhaegen PD, Van Zuijlen PP, Pennings NM, Van Marle J, Niessen FB, Van Der Horst CM, Middelkoop E. Differences in collagen architecture between keloid, hypertrophic scar, normotrophic scar, and normal skin: an objective histopathological analysis. Wound Repair Regener 2009;17:649–656.

Vinkel J, Holm NFR, Jakobsen JC, Hyldegaard O. Effects of adding adjunctive hyperbaric oxygen therapy to standard wound care for diabetic foot ulcers: A protocol for a systematic review with meta-analysis and trial sequential analysis. BMJ Open 2020;10 e031708.

Wilson BC, Adam G. A Monte Carlo model for the absorption and flux distributions of light in tissue. Med Phys 1983;10:824–830. [PubMed: 6656695]

Yabunaka K, Iizaka S, Nakagami G, Fujioka M, Sanada H. Three-dimensional ultrasound imaging of the pressure ulcer: A case report. Med Ultrasonogr 2015;17:404–406.

Yanez CO, Morales AR, Yue X, Urakami T, Komatsu M, Järvinen TA, Belfield KD. Deep vascular imaging in wounds by two-photon fluorescence microscopy. PLoS One 2013;8:e67559. [PubMed: 23844028]

Yudovsky D, Nouvong A, Pilon L. Hyperspectral imaging in diabetic foot wound care. J Diabetes Sci Technol 2010;4:1099–1113. [PubMed: 20920429]

Zamfirescu D, Owen E, Lascar I, Molitor M, Zegrea I, Popescu M, Bishop G, Lauer C, Simionescu M, Climov M. 2009 Sentinel skin allograft—A reliable marker for monitoring of composite tissue transplant rejection. Transplant Proc 2009;41:503–508. [PubMed: 19328913]

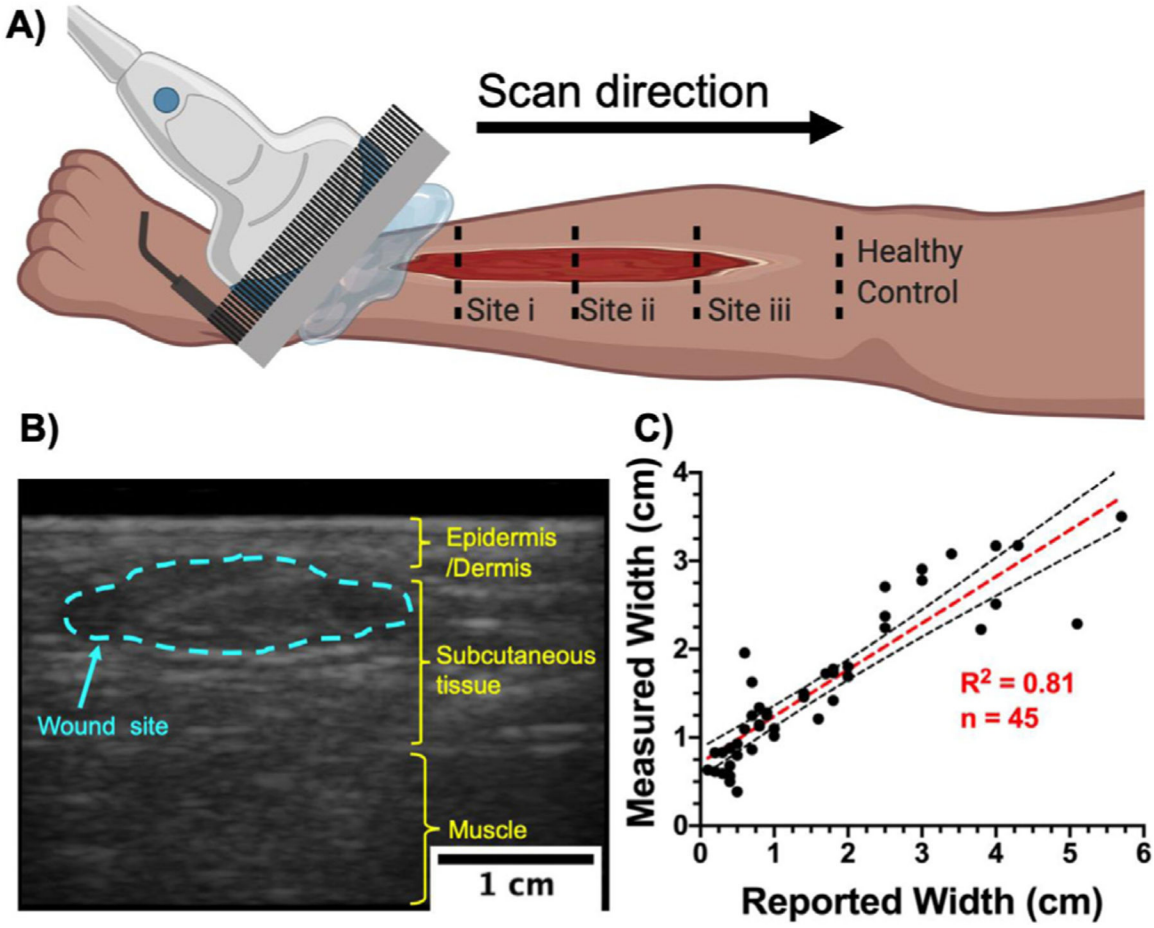

Fig. 1.

Ultrasound imaging setup and wound width measurement. (a) Schematic representation of a typical ultrasound scan over a wound site. Small wounds (<5 cm in length) were scanned in one sweep from inferior to superior healthy tissue. Large wounds were imaged at discrete distances from the inferior wound edge. Superior and inferior tissue from the wound edge were considered as healthy controls. (b) A typical B-mode US image revealing a coronal cross-section of the lower limb. Wound width was measured at its widest point within the wound site (*blue dotted line*). (c) Comparison between reported wound width at the point of care and wound width measured using US (n = 45) revealed a strong correlation ($R^2 = 0.81$, $p < 0.0001$) between the gold standard and our method. *Black dotted lines* represent 95% confidence intervals.

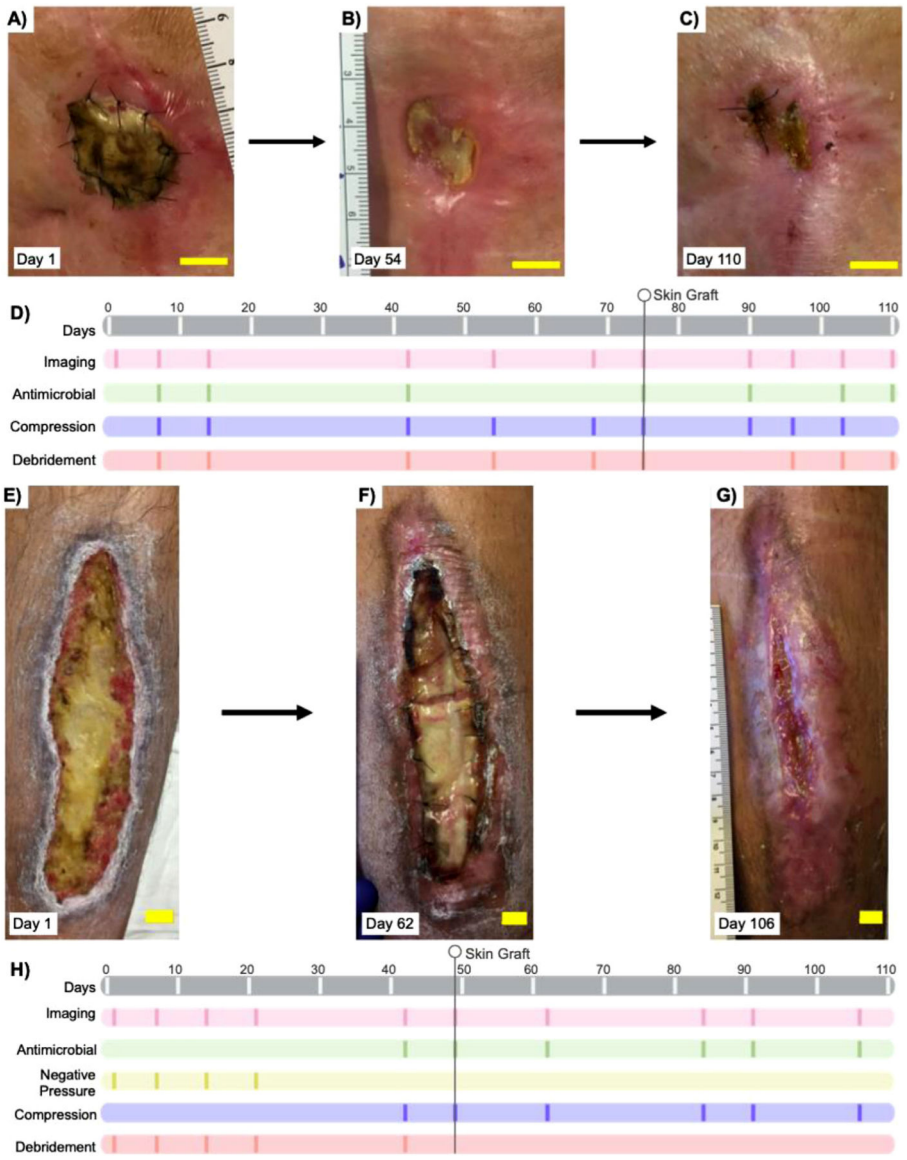

Fig. 2.

Study and treatment timeline. (a–c) Photographs of progression of the wound site in patient A, a 77-y-old woman with a chronic left knee wound. (d) Study and treatment timeline for patient A; 13 scans over a 110-d period. Patient A received two skin grafts, 28 d before and 75 d after the start of this study. (e–g) Photographic progression of the wound site in patient B, a 33-y-old man with a chronic, left lower limb wound. (h) Study and treatment timeline for patient B; 10 scans over a 106-d period. Patient B received a skin graft 49 d into the study. All bars = 2 cm.

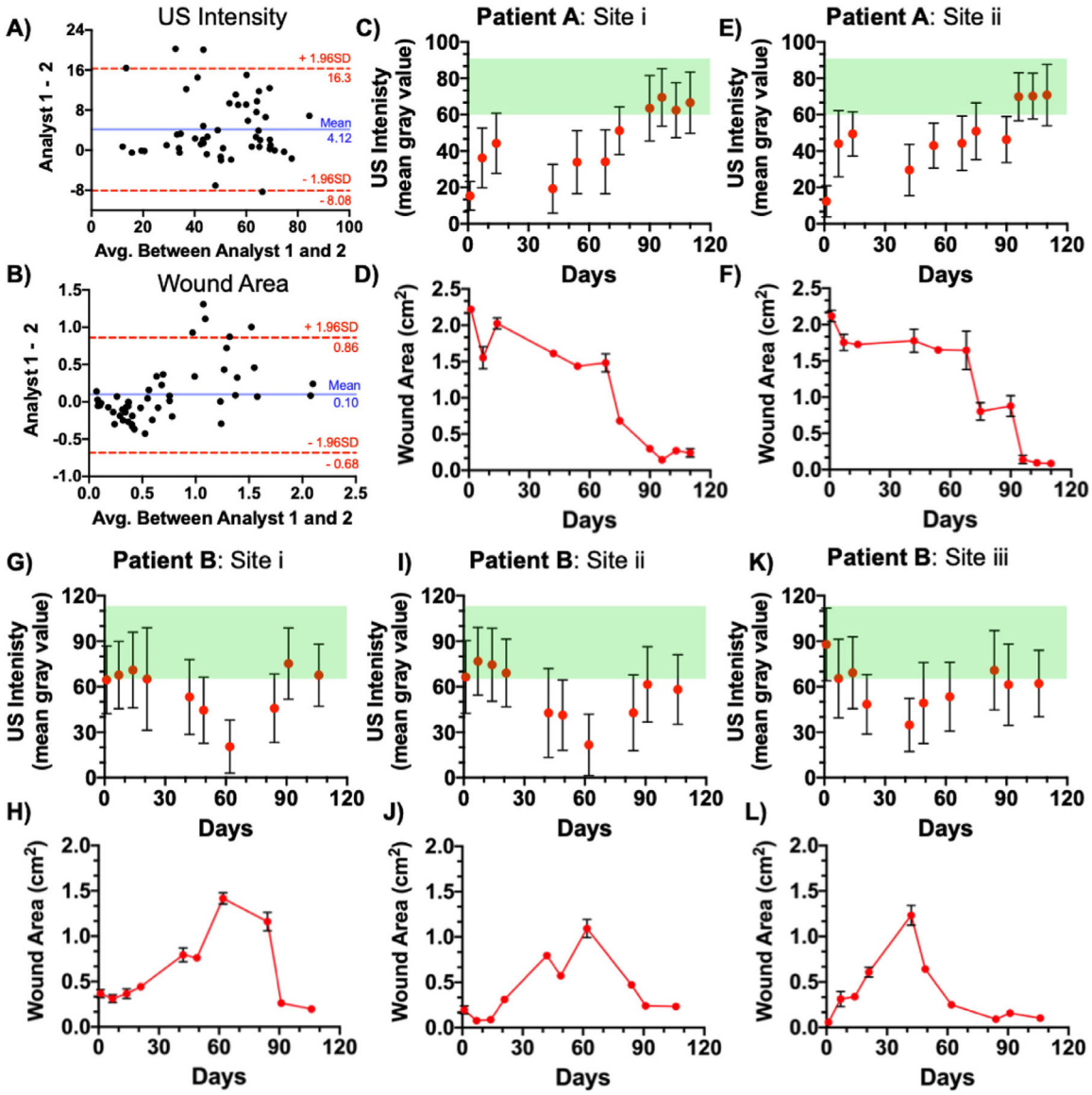

Fig. 3.

Wound size and intensity measurements. (a, b) Bland–Altman analysis between measurements made by two independent analysts using the same set of images. Statistical analysis of both US intensity (a) and wound area (b) revealed no significant bias between the two analysts. (c–f) Change in US intensity and wound area for patient A, sites i and ii. Sites i and ii exhibited 89.2% and 96.0% reductions in size, respectively. (g–l) Change in US intensity and wound size for patient B, with sites i, ii and iii exhibiting an 86.1%, 78.6% and 91.7% contraction, respectively. Error bars in panels c, e, g, i and k represent standard deviation of mean gray value in a single ROI. Error bars in panels d, f, h, j and l represent the standard deviation of area measured using three US frames. US = ultrasound.

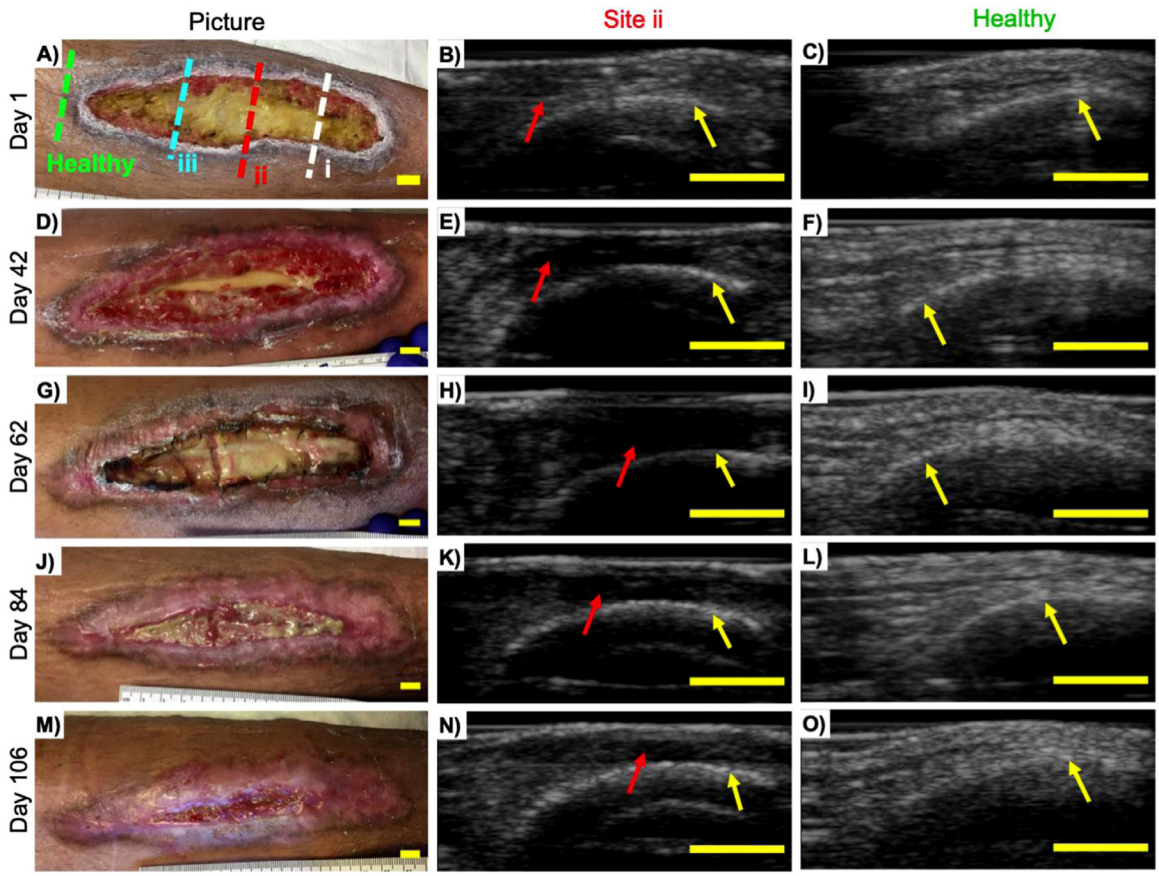

Fig. 4.

Monitoring wound progression using ultrasound. Patient B was a 33-y-old man with an anterior lower limb wound who received an allogenic skin graft 49 d into the study. Photographs and US images from Site ii (red dotted line) and superior healthy tissue (green dotted line) from (a–c) day 1, (d–f) day 42, (g–i) day 62, (j–l) day 84 and (m–o) day 106. Signs of tissue loss (b) can be seen using US while not visible to the eye (a). An increase in wound size and hypo-echoic regions were observed (b, e, h) over the first 62 d, indicating tissue loss even though skin grafting was done on day 49. An increase in echogenicity indicating tissue regeneration and wound contraction can be seen between days 62 and 106 (k, n). The ability to monitor tissue loss and regeneration under a skin graft between days 49 and 62 and days 62 and 106, respectively, illustrates the main power of imaging over current methods. Superior healthy control tissue (*green dotted line*) remains fairly unremarkable and unchanged over the same period. *Red arrows* point to wound site; *yellow arrows* point to the tibia. All bars = 1 cm. US = ultrasound.

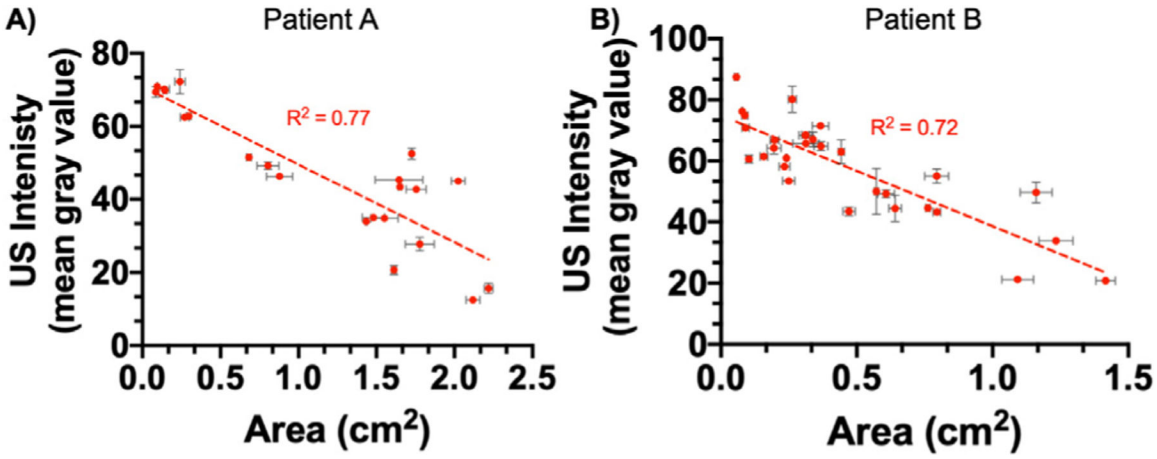

Fig. 5.

Relationship between wound size and US intensity. Wound size is negatively correlated to US intensity for both (a) patient A ($R^2 = 0.77$, $p < 0.0001$) and (b) patient B ($R^2 = 0.72$, $p < 0.0001$). As the skin graft takes, wound size decreases as healthy cells infiltrate the graft matrix. This infiltration results in tissue regeneration and an increase in US intensity. Error bars represent the standard error of the mean between three US frames. US = ultrasound.

Table 1.

Patient demographic distribution

Category	Distribution
Age (mean ± standard deviation)	66.9 ± 14.6
Male/female	31/32
Diabetic/non-diabetic	19/44
Chronic venous hypertension (yes/no)	37/26